Eur Biophys J (1994) 23: 337–348

European Biophysics Journal

Influence of obstacles on lipid lateral diffusion: computer simulation of FRAP experiments and application to proteoliposomes and biomembranes

Vincent Schram, Jean-François Tocanne, André Lopez

Laboratoire de Pharmacologie et Toxicologie Fondamentales du CNRS (Département III), 118 route de Narbonne, F-31062 Toulouse Cedex, France

Received: 4 May 1994 / Accepted: 30 August 1994

Abstract. Fluorescence Recovery After Photobleaching experiments were simulated using a computer approach in which a membrane lipid leaflet was mimicked using a triangular lattice obstructed with randomly distributed immobile and non-overlapping circular obstacles. Influence of the radius r and area fraction c of these obstacles and of the radius R of the observation area on the relative diffusion coefficient D^* (Eq. (1)) and mobile fraction M was analyzed. A phenomenological equation relating D^* to r and c was established. Fitting this equation to the FRAP data we obtained with the probe NBD-PC embedded in bacteriorhodopsin/egg-PC multilayers suggests that this transmembrane protein rigidifies the surrounding lipid phase over a distance of about 18 Å (≅two lipid layers) from the protein surface. In contrast, analysis of published diffusion constants obtained for lipids in the presence of gramicidin suggests that in terms of lateral diffusion, this relatively small polypeptide does not significantly affect the surrounding lipid phase. With respect to the mobile fraction M, and for point obstacles above the percolation threshold, an increase in R led to a decrease in M which can be associated with the existence of closed domains whose average size and diffusion properties can be determined. Adaptation of this model to the re-interpretation of the FRAP data obtained by Yechiel and Edidin (J Cell Biol (1987) 115:755–760) for the plasma membrane of human fibroblasts consistently leads to the suggestion that the lateral organization of this membrane would be of the confined type, with closed lipid domains of ≅0.5 μm^2 in area.

Key words: FRAP – Computer simulations – Percolation – Lipid lateral diffusion – Bacteriorhodopsin – Multilayers – Annular lipid domains – Lipid microdomains

Introduction

In the Fluid Mosaic Model of membranes, lipids are organized in the form of a bilayer supporting peripheral and integral proteins. This model considers the lipid bilayer as a two-dimensional fluid in which lipids and proteins are free to diffuse laterally (Bloom et al. 1991). As a direct consequence, both types of molecules would be expected to be randomly distributed within the membrane plane. In fact, if the concept of lipid bilayer is currently accepted, membrane organization is certainly much more complex. It is now well established that many membrane proteins are not free to diffuse, presumably owing to their attachment to cytoskeleton components (Cherry 1979) and that proteins act as obstacles to the lateral diffusion of lipids (Tocanne et al. 1994a and references herein). Furthermore, there is increasing evidence that lipids and proteins are not randomly distributed in biological membranes (Edidin 1987; Yechiel and Edidin 1987; Tocanne 1992) and that protein/lipid interactions play a key role in this membrane lateral organization (Thomas et al. 1994; Tocanne et al. 1994b). The relationships between the lateral distribution and the lateral diffusion of lipids in membranes have been investigated using a large variety of techniques (Tocanne 1992). This problem has also been investigated from a theoretical point of view with Monte-Carlo simulations of the diffusion of a point tracer in honeycomb (Saxton 1987, 1989a), square (Saxton 1987, 1992) or triangular (Eisinger et al. 1986; Saxton 1987, 1989b) lattices, obstructed with obstacles of various sizes and area fractions. Analytical treatments of self-obstructed diffusion have also been developed (Abney et al. 1989; Pink 1985; Saxton 1982; Scalettar and Abney 1991). In a recent paper, Almeida et al. (1992) have generalized the free-volume theory of lateral diffusion to a heterogeneous bilayer in

Abbreviations and notations used: BR, bacteriorhodopsin; DMPC, dimyristoylphosphatidylcholine; diOC18, dioctadecyloxatricarbocyanine; egg-PC, egg-yolk phosphatidylcholine; NBD-PC, 1-acyl-2-[12-[(7-nitro-2-1,3-benzoxadiazol-4-yl)amino]dodecanoyl]-sn-glycero-3-phosphocholine; MOPS, 3-[N-morpholino]propane sulfonic acid; FRAP, Fluoresence Recovery After photobleaching; D, observed diffusion coefficient; D_0, diffusion coefficient in the absence of obstacles; D^*, relative diffusion constant (Eq. 1); M, mobile fraction; c, obstacle area fraction; r, obstacle radius; R, observation area radius; r_d, diffusion area radius

Correspondence to: A. Lopez

which immobile circular obstacles are assumed to be surrounded by a few layers of lipids with a restricted free area (and therefore restricted diffusion) as compared to the bulk of the fluid lipid phase. As a main result, these various models show that for a given obstacle size, the relative diffusion constant D^* decreases nearly linearly with increasing obstacle area fractions and that for fixed area fractions, they become less efficient in slowing down lateral diffusion when the size of the obstacles grows (Almeida et al. 1992; Eisinger et al. 1986; Saxton 1989a, b, 1992).

Experimentally, long-range translational motions of lipids and proteins are conveniently measured by the widely used Fluorescence Recovery After Photobleaching (FRAP) technique, from which not only the diffusion coefficient D of the diffusing species can be determined but also their mobile fraction M (Axelrod et al. 1976; Vaz et al. 1982). When the radius R of the illuminated area is small as compared to the radius r_d of the diffusion area ($r_d/R>5$, condition of an infinite reservoir) and for freely diffusing species, M must be nearly equal to 100% (Lopez et al. 1988). In fact, most of the FRAP data reported so far for lipids (with the condition of an infinite reservoir being satisfied) show the existence of an immobile fraction which, today, can be considered as one of the best indications that lipid domains exist in biological membranes (Tocanne 1992).

However the mobile fraction is not accessible when the above theoretical approaches are used. To obtain this parameter directly and to further elucidate the relationships between lipid dynamics and membrane lateral organization, it was interesting to simulate FRAP experiments in obstructed lipid bilayers. We present here the results of such simulations carried out in a triangular lattice of point tracers obstructed with obstacles of various sizes and area fractions and their application to the experimental FRAP data we obtained with the probe NBD-PC embedded in egg-PC multilayers incorporating the transmembrane protein bacteriorhodopsin, and also to FRAP data published in the literature.

Materials and methods

Chemicals

Egg yolk phosphatidylcholine (egg-PC) was obtained from Sigma Chemical Co., (St. Louis, MO). The fluorescent probe 1-acyl-2-[12-[(7-nitro-2-1,3-benzoxadiazol-4-yl) amino] dodecanoyl]-sn-glycero-3-phosphocholine (NBD-PC) was purchased from Avanti Polar Lipids, Inc. (Birmingham, AL). All lipids were checked for purity by thin-layer chromatography and stored at –20 °C as dry material or as chloroform solutions for short periods. All other chemicals were of analytical grade. Bacteriorhodopsin, in the form of water suspension of the purple membrane purified from the bacterium *Halobacterium halobium* (Oesterhelt and Stoeckenius 1974), was kindly provided by Dr. J. L. Ranck (Centre de Génétique Moléculaire, CNRS, Gif-sur-Yvette, France). The purple membrane was used without delipidation, for the reconstitution of bacteriorhodopsin with egg-PC. Standard buffer was: 5 m*M* MOPS, 10 m*M* NaCl, pH=7.

Preparation of hydrated BR/egg-PC multilayers

For the reconstitution of BR into egg-PC vesicles, the method based on spontaneous incorporation of integral membrane proteins into preformed lipid bilayers was used (Scotto and Zakim 1988).

The required amount of a chloroform solution of 0.5 mol% NBD-PC in egg-PC was dried under a nitrogen stream at a temperature of 40 °C and then for 1 h in vacuum. Distilled water (1 ml) was added and the sample was vortexed (1 min) and then sonicated (sonicating bath, 15 min) until small unilamellar vesicles were obtained. The desired amount of aqueous suspension of BR (in the form of the purple membrane) was added to this phospholipid sample, and the medium was sonicated again for 30 s and incubated overnight at 30 °C.

Reconstituted BR/egg-PC vesicles were checked for composition and homogeneity by recording the absorption spectrum of retinal and by ultracentrifugation of the proteoliposomes on a linear sucrose density gradient (5%–40%) as already described (Heyn and Dencher 1982). In these preparations, the absorption spectrum of retinal was as expected, both in shape (maximum absorption wavelength of 550 nm) and intensity. Only one purple band was observed on the sucrose gradient, superimposed on the lipid band (determined through phosphorus analysis).

To determine the area fraction of BR in the bilayer, it was necessary to take into account the presence of about 10 endogenous lipids which accompany each protein molecule (Blaurock 1975). For these calculations, molecular areas of 690 $Å^2$ for BR (Henderson and Unwin 1975), 75 $Å^2$ for the endogenous lipids (Blaurock 1975) and 50 $Å^2$ for egg-PC were used. The amount of BR was determined spectroscopically (molecular extinction coefficient of 63 000 dm^3/mol/cm at 570 nm and 20 °C). Proteoliposomes with protein area fractions ranging from 0 to 0.6 were prepared.

Note that the fluorescence of the NBD fluorophore decreased regularly with increasing protein concentration. This can originate: (i) from fluorescence energy transfer from NBD as donor to retinal as acceptor, as already described for the fluorescent probe DPH (Rehorek et al. 1985); (ii) from the fact that in proximity of the protein, the NBD group can experience a more rigid lipid environment which in turn will promote its motion from the hydrophobic lipid core toward the more polar water/lipid interface, with a considerable decrease of its fluorescence quantum yield (Fery-Forgues et al. 1993).

The volume of the proteoliposome suspension was reduced to 20 µl by gentle evaporation and the preparation was deposited on a glass slide. Water was removed first by gently drying the sample under a nitrogen stream (two hours) and then in vacuum for 30 min. Finally, the preparation was rehydrated by addition of 70 µl of buffer. Proteoliposomes were covered by a coverslip, compressed

to 60 N/cm^2, further incubated at 20 °C for 24 h in water-saturated atmosphere and sealed with paraffin wax to prevent dehydration. This procedure yielded flat multilayer domains large enough for FRAP experiments (at least 20 µm in radius), for BR area fractions not exceeding 0.4.

FRAP experiments

FRAP experiments were carried out under conditions of constant incident light intensity and of "uniform disk illumination" using an apparatus of our fabrication (Lopez et al. 1988). A Leitz X63/1.3 oil (n=1.52) immersion-objective was used. The radius of the illuminated area was 4.2 µm, compatible with the radius of at least 20 µm of the diffusion area (condition of infinite reservoir) (Lopez et al. 1988). Bleached fractions of 35–45% were obtained for a bleaching time of 150 ms. This time was consistent with the approximate 2 s recovery half-time currently found in the BR/egg-PC samples. At least 30 recoveries where recorded for each sample at a temperature of 20 °C.

Analysis of FRAP data

For both experimental and simulated FRAP experiments, the diffusion coefficient D and the mobile fraction M were obtained by double fitting of the recovery data, using the classical equation of diffusion (Axelrod et al. 1976; Lopez et al. 1988 and references cited herein). A minimization algorithm and statistical analysis were developed which, by using the whole set of recovery data obtained for a certain number of FRAP measurements, provided the solution value for D and M and their minimum (D_{min}, M_{min}) and maximum (D_{max}, M_{max}) values (Lopez et al. 1988). In the present work, the D and M values are given at a 95% confidence level.

In order to compare our results with other works and consider the effect of obstacle radius and area fractions, the diffusion coefficients are presented in the standard form (Saxton 1987, 1989b, 1992):

$$D = D_0 D^*_{(r,c)} \quad (1)$$

in which D is the diffusion coefficient obtained from experimental or simulated recoveries, D_0 is the diffusion coefficient in the absence of obstacles and $D^*_{(r,c)}$ is the dimensionless relative diffusion constant which depends on the obstacle radius r and area fraction c and which is normalized at 1 to c=0. For the sake of clarity, $D^*_{(r,c)}$ will be noted D^*.

Analysis of FRAP experiments and FRAP simulations were carried out with a 486 PC clone computer. The programs were written in Basic language (Professional Development System, Version 7.0, Microsoft corporation). For the simulation of random walks, the subroutine for the generation of random numbers of a language was used twice to avoid any non-random effects.

Results

1. Simulated FRAP experiments

a. Influence of obstacle area fraction c and observation area radius R on D and M for point obstacles.* Our approach for simulating FRAP experiments is described in Appendix A.

In an obstacle-free lattice, calculated D^* values were found to be nearly independent of the observation area radius R (D^*=0.915, 1.000, 0.985, 1.006, 0.954 and 0.911 for R=7, 10, 15, 20, 25 and 28 lattice spacings respectively).

In the presence of point obstacles and for each R value used, D^* was observed to decrease nearly linearly when increasing the obstacle area fraction c over the range 0–0.4 (Fig. 1 A). In this case, R still had only slight influence on D^*. For each R value tested, the corresponding D^* versus C plots extrapolated at D^*=0 for c around 0.5, which is the expected value of the percolation threshold c_p for a triangular two-dimensional lattice (Stauffer and Aharony 1992). These D^* and c_p values agree with those previously reported by Saxton (1987; 1989b) for point obstacles distributed over a triangular lattice (see the straight line in Fig. 1 A) and which were obtained using a somewhat different approach in which D^* was computed from the mean-square displacements $\langle r^2 \rangle$ of the tracers.

For $c \geq 0.5$, i.e. above the percolation threshold, and as already reported by Almeida et al. (1992), D^* was found to increase with c and R (see insert in Fig. 1 A). In fact,

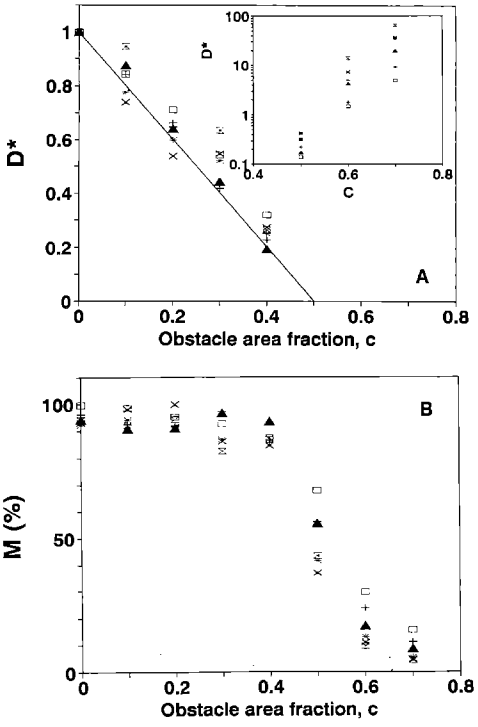

Fig. 1. Influence of the area fraction c of immobile point obstacles on the relative diffusion constant D^* **A** and mobile fraction M **B** of tracers for an observation area radius R of 7 (□), 10 (+), 15 (▲), 20 (×), 25 (x) and 28 (*) lattice spacings, and for obstacle area fraction c<0.5. Insert shows the D^* values obtained for c>0.5. The straight line corresponds to the D^* values calculated by Saxton (1987b) for immobile point obstacles in a triangular lattice

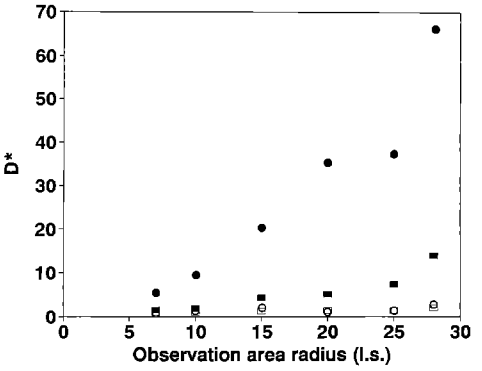

Fig. 2. Influence of the observation area radius R on the calculated values of the relative diffusion constant D^* for area fractions of 60% (■, □) and 70% (●, ○) of point obstacles. The full symbols show the apparent D^*_{app} values which are obtained when the full area of the observation area is accounted for in the calculation of D^* from the tracer recoveries. The open symbols show the actual D^*_0 values obtained from the corresponding D^*_{app} values and Eq. (2B) (Appendix B). These D^*_0 values are close to unity as expected for tracers diffusing freely in closed cavities, in the absence of obstacles

and as demonstrated in Appendix B, the tracers are now confined in closed cavities in which they diffuse at the nominal value $D^* \approx 1$, found in the absence of obstacles, independently of c and R. D^* increases because in fitting the recovery curves, diffusion is assumed to occur over the entire bleached area, when in fact it occurs within the closed cavities at the edge of the bleached area, and these cavities become smaller and smaller as c increases. As shown in Fig. 2, D^* regains its nominal value of ≈ 1, independent of c and R, when this reduction in diffusion area is accounted for.

The mobile fraction M remained close to 100% and nearly independent of R and c for $c \leq 0.4$ (Fig. 1B). Note that the uncomplete recoveries of ~93–97% observed for $R \geq 10$ l.s. do not account for immobile lipid fractions. They simply originate from the finite size of the system and the bleaching conditions used which led to the destruction of about 3–7% of the tracers introduced at the beginning of each FRAP simulation. For $c > 0.4$, M started to decrease regularly down to reach a value of 0.1 at $c = 0.7$. Slight dependence on R was also observed, the lowest mobile fractions found for a given obstacle area fraction being associated with the highest R values. As shown in Appendix B, these changes in M with R and c are also due to the existence of the closed cavities which exist above the percolation threshold. It is also shown that the average value of the radius r_m of these closed cavities can be evaluated from the product of M by R (3B).

To conclude this section, it is worth stressing that in the interpretation of the fluorescence recovery curves obtained from FRAP experiments carried out on a natural membrane, the diffusions coefficients are calculated by using the actual radius R of the illuminated area, without any assumption as to the lateral organization of the membrane. In other words, and if the condition of an infinite reservoir is satisfied, a concomitant increase in D and decrease in M with increasing R can indicate that closed lipid domains exist in that membrane, whose the average size may be estimated. Consequences of this important remark will be discussed below in Sect. 2 of the discussion.

b. Influence of obstacle area fraction c and observation area radius R on D and M for multi-site obstacles.* In these simulations, R was kept constant to 10 lattice spacings and the obstacle radius r took values of 1.5 l.s., 3.4 l.s., 5.3 l.s., 7.0 l.s., 9.4 l.s. and 13.8 l.s. corresponding to obstacle sizes of 7, 37, 87, 153, 279 and 595 sites respectively. Results are shown in Fig. 3A–E. With the exception of the obstacle concentration $c = 0.1$ in which D^* showed no significant dependence on r, multi-site obstacles became less efficient at slowing down lateral diffusion as they grew in size and this effect was more pronounced as c increased. As can be seen in Fig. 3C and as already noted for point obstacles, these simulated D^* values compared well with those obtained by Saxton (1989b) and Eisinger et al. (1986) for multi-site obstacles in a triangular lattice. The mobile fraction M remained close to unity and practically independent of r.

c. Quantification of simulated FRAP data for point and multi-site obstacles. For each r value tested and in agreement with documented data (Almeida et al. 1992; Eisinger et al. 1986; Saxton 1987, 1989b, 1992), D^* was found to decrease linearly with c (correlation coefficient r^2 better than 0.971), an observation which can be accounted for by the linear function:

$$D^* = 1 - a(r)\, c \tag{2}$$

in which $a(r)$ is the slope of the straight line found for a given value of r, expressed in lattice spacing units.

Now, but without real theoretical justification, $a(r)$ was observed to decrease linearly with the logarithm of r and best-fit linear adjustment ($r^2 = 0.982$) was achieved with the function:

$$a(r) = 1.574 - 0.475 \ln(r) \tag{3}$$

Combining Eqs. (2) and (3) leads to the phenomenological Eq. (4) which allows us to predict the value of the relative diffusion constant D^* for given values of r and c:

$$D^* = \{1 - [1.574 - 0.475 \ln(r)]\, c\} \tag{4}$$

For the measured diffusion coefficients, Eq. (4) is replaced by the expression:

$$D = D_0 \{1 - [1.574 - 0.475 \ln(r)]\, c\} \tag{5}$$

in which D_0 is the diffusion coefficient in the absence of obstacle. Note that in this equation, the lattice spacing unit for r is now to be referred to the size of the lipid molecules. Note also that Eqs. (4) and (5) are valid for $0.5 \leq r \leq 27$ lattice spacings and $c < 0.55$. For $r > 27$ lattice spacings, D^* values would exceed 1, which is not acceptable. For $c > 0.55$, overlap between randomly distributed obstacles would occur (Onoda and Liniger 1986).

2. Lateral diffusion in multilayers of bacteriorhodopsin/egg-yolk phosphatidylcholine

To study the influence of transmembrane proteins as obstacles to the lateral diffusion of lipids, bacteriorhodopsin

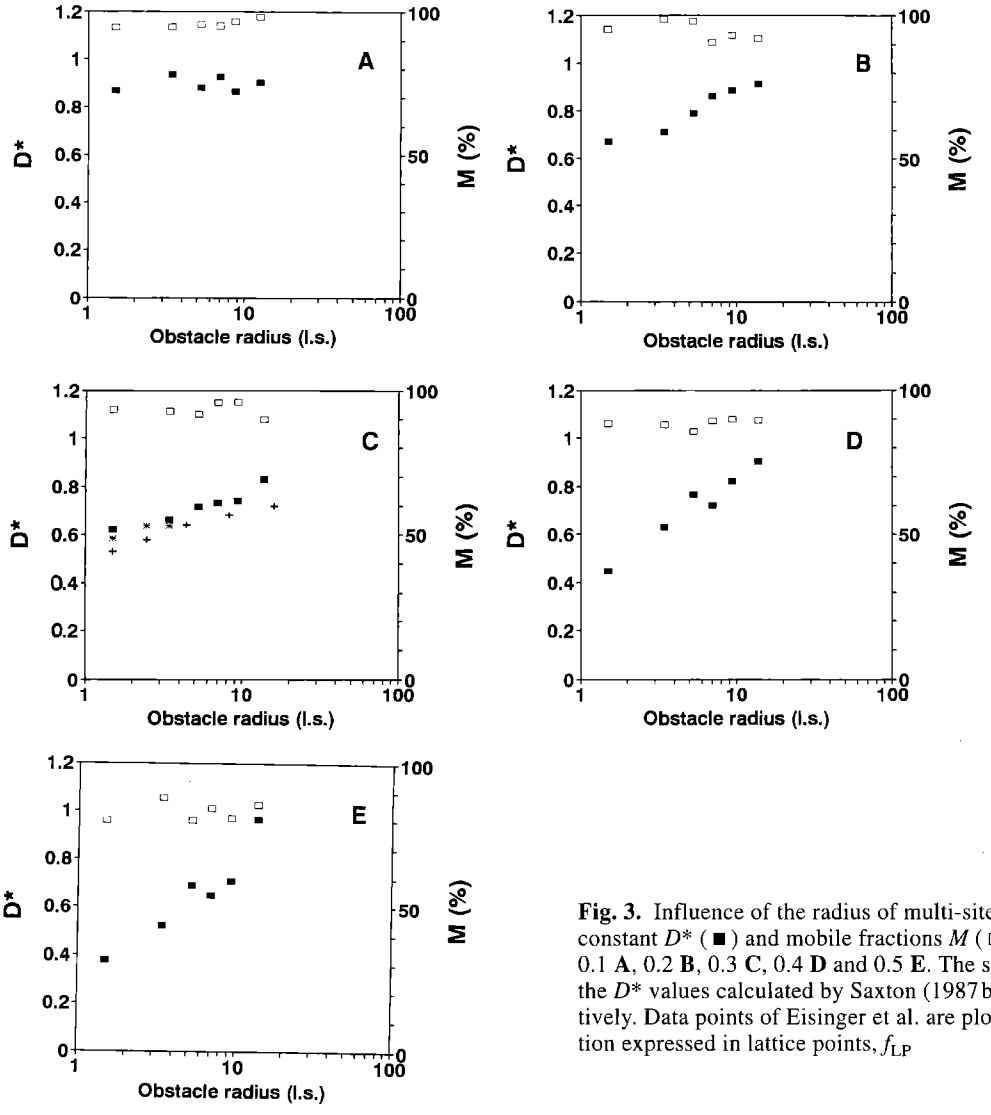

Fig. 3. Influence of the radius of multi-site obstacles on the relative diffusion constant D^* (■) and mobile fractions M (□) for obstacle area fractions of 0.1 **A**, 0.2 **B**, 0.3 **C**, 0.4 **D** and 0.5 **E**. The symbols + and × in **C** correspond to the D^* values calculated by Saxton (1987b) and Eisinger et al. (1986) respectively. Data points of Eisinger et al. are plotted against the obstacle area fraction expressed in lattice points, f_{LP}

from the bacterium *Halobacterium halobium* was used. This protein is structurally well known and can easily be purified and reconstituted in many kinds of lipids (Lewis and Engelman 1983). Multilayers of egg-yolk phosphatidylcholine incorporating the fluorescent probe NBD-PC and various amounts of BR were analyzed by FRAP experiments. As can be seen in Fig. 4, the diffusion coefficient of the probe decreased by a factor of 10 when BR area fractions increased from 0 to 0.3, above which value D remained nearly constant. In the full protein concentration range explored, the mobile fraction did not vary and was close to the 100% (not shown). The diffusion coefficients measured by Peters and Cherry (1982) for the probe diOC18 in BR/DMPC multilayers and extrapolated in Arrhenius plots at 20 °C are in excellent agreement with our own values (Fig. 4, full squares). This suggests that the various diffusion coefficients shown, obtained for different experimental conditions of fluorescent probe structure, reconstitution procedure and FRAP technique, can be considered as characteristic of the system studied.

Discussion

Direct computer simulations of FRAP experiments under conditions of uniform disk illumination have enabled us to examine the influence of the size and area fractions of immobile and non-overlapping randomly distributed circular obstacles on the diffusion coefficient D and the mobile fraction M of lipids in a membrane-like lattice. A phenomenological equation relating D and the obstacle radius and area fraction was established and we have shown that when diffusion is confined in closed cavities, the average size of these cavities can be estimated from the size of the observation area and the corresponding mobile fraction. We will examine the consequences of these simulations successively.

1. Interpretation of lipid diffusion coefficient data: lipid domains around bacteriorhodopsin

The phenomenological equation (5) can be applied to the experimental FRAP data obtained with bacteriorhodop-

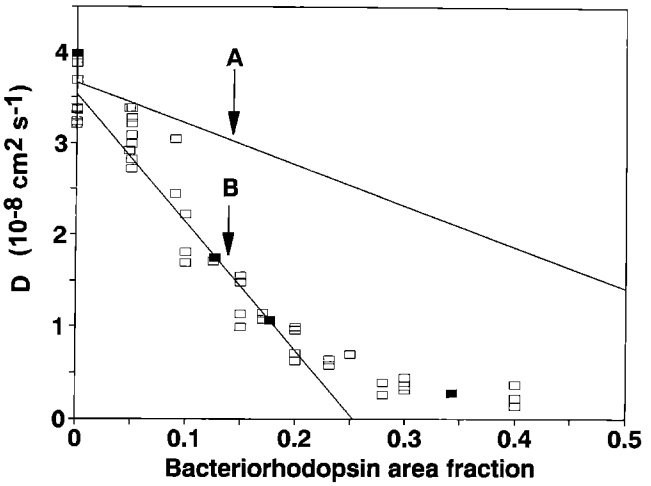

Fig. 4. Measured diffusion coefficients for the probe NBD-PC in bacteriorhodopsin/egg-PC planar multilayers for various protein area fraction. Each point (□) results from the global analysis of 30 recoveries in one multilayer. The closed symbols (■) correspond to the D values obtained by Peters and Cherry (1982) for the probe diOC18 in BR/DMPC multilayers and extrapolated at the temperature of 20 °C on Arrhenius plots. Line A is the best fit of (5) to the experimental data from $c=0$ to $c=0.2$, with $D_0=3.66\ 10^{-8}$ cm^2/s and a protein radius $r=15$ Å. Line B is the best fit of (7) to the experimental data from $c=0$ to $c=0.2$, with $D_0=3.66\ 10^{-8}$ cm^2/s, $r=15$ Å and $d=18$ Å

sin/egg-PC multilayers at the condition that the size of the obstacles to lipid diffusion is known. In the native purple membrane, bacteriorhodopsin is organized in a two dimensional hexagonal lattice of protein trimers (Henderson and Unwin 1975). The changes in the protein aggregation state resulting from dilution in exogenous lipids have been extensively investigated in many kinds of lipids (Lewis and Engelman 1983). In the case of egg-PC, one can reasonably assume that BR exists principally in the monomeric state for BR/egg-PC molar ratios less than 1/100 (Gulik-Krzywicki et al. 1987; Heyn et al. 1981), which corresponds to a protein area fraction of about 0.2. As a monomer, bacteriorhodopsin is elliptical (axes of 25 Å and 35 Å) with a molecular area of 690 Å^2 (Henderson and Unwin 1975). However, the protein can be approximated as a cylinder of 15 Å radius which corresponds to a radius of 2 lattice spacings if one assumes a molecular area of 50 Å^2 for egg-PC and therefore a lipid distance of 7.5 Å. In these conditions, fitting of (5) to the diffusion coefficients measured over the protein concentration range 0–0.2 yielded a quite acceptable value of 3.53 10^{-8} cm^2 s^{-1} for D_0 but led to line A in Fig. 4 which strongly deviated from the measured diffusion coefficients.

One possibility for fitting (5) to the data in Fig. 4 was to consider that the effective size of the obstacles was greater than that used. Because BR is a monomer over the concentration range 0–0.2, protein aggregation can be discarded and another alternative is to assume that BR was surrounded by a few layers of partially immobilized lipids. Indeed, it is now well established that through nonspecific long-range interactions, the acyl chains of lipids in contact with transmembrane proteins can be rigidified (Lentz 1988; Yeagle 1988; Marsh and Watts 1988). Such rigidification, which was demonstrated to occur with bacteriorhodopsin (Heyn et al. 1981; Piknova et al. 1993; Rehorek et al. 1985), is expected to further decrease the overall translational diffusion of lipids. Although the influence of the protein on the lipids is expected to decay exponentially from its surface with a characteristic coherence length ξ (Jähnig 1981; Owicki et al. 1978; Sperotto and Mouritsen 1988, 1991; Piknova et al. 1993; Almeida et al. 1992), consequences of these protein/lipid interactions on lipid diffusion can be approximated in a first step by considering each protein molecule as being surrounded by a shell of immobilized lipids of thickness d. Then, the radius of the new obstacle becomes $r+d$ and its area fraction c_{ob} is:

$$c_{ob} = c\,\frac{(r+d)^2}{r^2} \tag{6}$$

Combining Eqs. (5) and (6), one obtains:

$$D = D_0\left[1-[1.574-0.475\ln(r+d)]\,c\,\frac{(r+d)^2}{r^2}\right] \tag{7}$$

Good fitting of (7) to the diffusion coefficients measured over the protein concentration range 0–0.2 lead to line B in Fig. 4 and was achieved for $D_0=3.66\ 10^{-8}$ cm^2 s^{-1} and $d=18\pm3$ Å. A thickness of 18 Å corresponds to 2.4 layers of immobilized lipids for a distance of 7.5 Å between lipid molecules. It is interesting to note that line B extrapolated at $D=0$ for a protein area fraction of 0.25. This is the value up to which bacteriorhodopsin can be reasonably considered as a monomer in the host lipids (Gulik-Krzywicki et al. 1987; Heyn et al. 1981). Above this threshold concentration, the protein is expected to aggregate and to form very large obstacles. According to the above FRAP simulations and those from Eisinger et al. (1986) and Saxton (1989b), an increase in obstacle area fraction would then be compensated by an increase in obstacle size, thus explaining the small variations in D which were observed for protein area fractions above 0.25 (Fig. 4).

As mentioned in the Introduction, Almeida et al. (1992) have recently proposed a theoretical treatment of the effects of immobile and rigid circular obstacles on translational diffusion, which is based on the free-volume theory of diffusion and which takes into account long-range lipid/protein interactions and their exponential decay away from the protein surface. By calculating the diffusion coefficient from a two-dimensional integration of the relative free area around randomly distributed obstacles, an analytical expression relating the relative diffusion constant D^* to the obstacle size and area fractions was obtained. Fitting of this expression to the data in Fig. 4, over the protein concentration range 0–0.2, was achieved with a coherence length $\xi=11\pm4$ Å, also suggesting the existence of a shell of partly immobilized lipids around the protein. It should be stressed that intrinsically, d and ξ are distinct parameters which are not expected to take the same value. However, the values of 18 Å and 11 Å found respectively for these two parameters are quite compatible. Indeed, $\xi=11$ Å means that the influence of the protein ex-

tends significantly (80%) over three to four lipid layers, a distance which encompasses the two lipid layers corresponding to $d = 18$ Å.

It should be noted that these two simulations consider immobile obstacles, an assumption which is not strictly met when working with integral membrane proteins reincorporated in lipid bilayers. However, in fluid DMPC multilayers, bacteriorhodopsin was shown to diffuse laterally, at a rate about one third that of the lipids for a protein/lipid ratio of 1/210, which decreased to one sixth for the 1/90 ratio (Peters and Cherry 1982). It is worth noting that this decrease in protein diffusivity with increasing protein concentration is a general phenomenon which originates from various factors, in particular obstruction and hydrodynamic interactions (Abney et al. 1989; Scalettar and Abney 1991; Bussell et al. 1994). The fact that the protein is not completely immobile makes an exact determination of the thickness of the perturbed lipid shell difficult when one or the other of the two above simulations is applied to experimental results. However, these remarks do not modify the conclusion that the protein is surrounded by a shell of partly immobilized lipids. On account of the observation that mobile obstacles are less efficient in slowing down lateral diffusion than immobile ones (Saxton 1987), the thickness of this shell, as deduced from the parameters d and ξ of 18 Å and 11 Å, is probably slightly underestimated. On the other hand, direct protein-protein interactions which probably occur when protein area fractions increase may reduce D and therefore the estimated value of d. Anyhow, these d and ξ values are consistent with the ξ value of 12 Å used to account for the upward shifts in lipid phase transition temperature provoked by bacteriorhodopsin when reincorporated into dilauroylphosphatidylcholine vesicles (Piknova et al. 1993). These d and ξ values are compatible with the observation obtained through time resolved fluorescence polarization and energy transfer experiments between the probe diphenylhexatriene and the retinal of bacteriorhodopsin, that the influence of the protein extends beyond a distance of 45 Å (6 lipid layers) in the lipid phase (Rehorek et al. 1985). In accordance with these deductions obtained for bacteriorhodopsin, we noted that a coherence length of 15 Å was proposed by Jähnig (1981) from theoretical considerations, to account for long-range protein/lipid interactions in membranes. The same value was also conveniently used for quantifying the shifts of lipid phase transition temperature induced by the reaction center proteins of *Rhodopseudomonas spheroides* incorporated in ditridecanoyl-phosphatidylcholine vesicles (Peschke et al. 1987).

Our simulations were also applied to published data concerning the effects of gramicidin on the lateral diffusion of lipids. They were obtained either through FRAP experiments in the presence of gramicidin C (Tank et al. 1982) or by measuring the fluorescence quenching of pyrene by plastoquinone in the presence of gramicidin D (Blackwell and Whitmarsh 1990). Note that the differences in D values which are observed presumably originate from differences in length-scales between the two approaches (Tocanne et al. 1994a). The transmembrane area of gramicidins can reasonably be approximated by a circle of 8 Å in radius (Wallace and Ravikumar 1992). Still

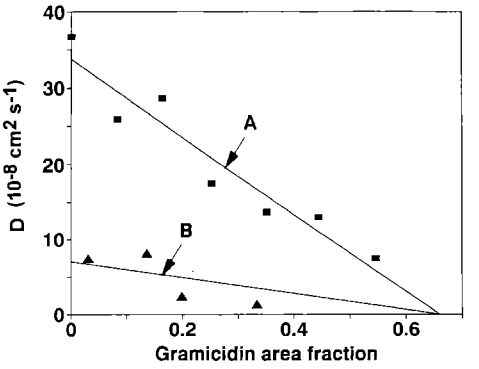

Fig. 5. Influence of gramicidin on the diffusion coefficient of lipids in reconstituted systems. (■): data of Blackwell and Whitmarsh (1990). D was obtained by following the fluorescence quenching of pyrene by plastoquinone in gramicidin D/soybean phosphatidylcholine vesicles. (▲): data of Tank et al. (1982). D was measured through FRAP experiments for the probe NBD-PE in gramicidin C/DMPC multilayers. Lines A and B show the best fitting of (5) to the diffusion data using a radius r of 8 Å for gramicidin. D_0 was found to have a value of 33.9 10^{-8} cm^2/s for the data of Blackwell and Whitmarsh and of 7.0 10^{-8} cm^2/s for the data of Tank et al.

using a molecular area of 50 $Å^2$ for the lipids, good fitting of (8) to the data of Blackwell and Whitmarsh (Fig. 5, line A) and Tank et al. (Fig. 5, line B) was achieved without taking into account an annular domain of rigidified lipids, indicating that in terms of lipid lateral diffusion, gramicidin does not induce a rigidification of the surrounding lipid phase. The same behavior has already been reported (Almeida et al. 1992; Blackwell and Whitmarsh 1990) and was attributed to the small size of this peptide which diffuses laterally at a rate similar to that of the surrounding lipids (Tank et al. 1982).

2. Interpretation of lipid diffusion coefficient and mobile fraction data: lipid microdomains in membranes

Another consequence of our FRAP simulation is that if closed lipid domains exist in a biological membrane, it should in principle be possible to recognize their existence and to evaluate their average size with (2B) and (3B) derived in Appendix B and the various D and M values obtained from FRAP experiments carried out with varying the radius R of the illuminated area.

There is one report of such FRAP data obtained for the lipid probe NBD-PC in the plasma membrane of human fibroblasts (Yechiel and Edidin 1987). Increases in D and decrease in M with increasing beam radius R were observed which were interpreted as reflecting the existence of protein-rich domains about 1 μm in diameter, embedded in a relatively protein-poor lipid continuum. Fibroblastic cells have an average diameter around 15–30 μm (Yechiel and Edidin 1987). This means that for beam radius R in the range 0.325 μm–5 μm, the condition of an infinite reservoir was always satisfied. In fact, these changes in D and M with R are reminiscent of what we described in the case of point obstacles above the percolation threshold, when diffusion is confined in closed cav-

ities. By extension of this model, these FRAP data can be re-interpreted in a self-consistent way by considering now the membrane as a system in which the diffusion of lipids (and proteins) is confined to closed domains separated by fences. This view is supported by recent data obtained by means of particle tracking and laser tweezer techniques which show that the lateral diffusion of receptor molecules in the plasma membrane of rat kidney fibroblastic cells is of the confined type. The boundaries or fences between domains would be made of dynamically fluctuating membrane skeletons (Kusumi 1994).

In such a model of lateral organization of membranes, the area fraction of the fences can be considered as negligible and therefore the mean diffusion coefficient can be obtained from the simplified form of (2B):

$$D_0 = 2\, r_m\, D_{app}/R \qquad (8)$$

in which equation, D_{app} is the measured diffusion coefficient and D_0 is the intrinsic diffusion coefficient in the closed domain. The average radius r_m of the domains is considered as a constant and can be estimated by using (3B) in Appendix B. One could argue that (3B), which was deduced for the condition of uniform disk illumination, cannot be used for the interpretation of FRAP data obtained with a laser beam. In fact, as shown by Axelrod et al. (1976) and due to the high energy of the bleaching pulse, the radial distribution of bleached fluorophores in the illuminated area is trapezoïdal and not Gaussian, and is not very different from that observed when the condition of uniform disk illumination is used (Lopez et al. 1988).

Under this approximation and according to this model of membrane lateral organization, M should vary linearly with $1/R$ while D_0 should remain constant, independent of R. Indeed, applying (3B) to the mobile fractions reported by Yechiel and Edidin (1987) for different beam radius R yielded the plot in Fig. 6A which shows a linear increase of M with $1/R$ ($r^2=0.973$). From this plot, a value of 0.4 μm was calculated for r_m, corresponding to a domain of 0.5 μm^2 in area. Note that (3B) can be used only if the condition $R > r_m$ is satisfied. For that reason, the data related to the very small beam radius of 0.35 and 0.4 μm were discarded. After reporting the r_m value of 0.4 μm in (8) and calculating D_0 from the reported D_{app} and R values, the plot in Fig. 6B shows that within the experimental error, D_0 remained independent of R, with a quite acceptable value of 1.5 10^{-9} cm^2/s. It is thus interesting to note that despite the various approximations used, this approach provides a new and self-consistent description of the lateral organization of the plasma membrane of the human fibroblasts investigated by Yechiel and Edidin (1987) which thus might be of the confined type. Lipid domains of 0.5 μm^2 in surface do not seem unrealistic and they resemble those of 0.225 μm^2 (0.5–0.7 μm in diagonal length) proposed by Kusumi (1994) to describe the plasma membrane of rat kidney fibroblasts. It is clear that this kind of investigation should be further extended to other probes and cell membranes.

To conclude, our simulations of the lateral motion of lipids in the presence of obstacles have proved to be useful for obtaining information on the influence of transmembrane proteins on the lateral diffusion of lipids and also structural data on the cross-sectional area of transmembrane proteins and the presence or absence of an annular domain of partly rigidified lipid molecules around them. The simulations show that a mobile fraction M of less than 100% can be due to lateral compartmentalization of the diffusion plane, and that the size r_m of these domains is directly related to M and the radius R of the observation area. Our results shed a new light on the potential of FRAP experiments, when coupled with theoretical analysis of the data, in investigating membrane lateral heterogeneities and providing some clue as to the structure of lipid microdomains in membranes.

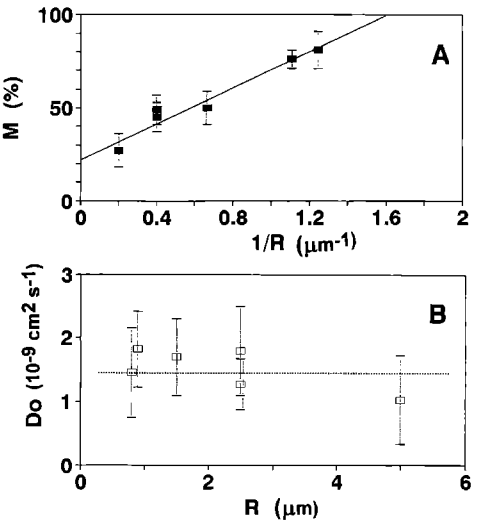

Fig. 6. Panel **A** shows that the mobile fractions M measured by Yechiel and Edidin (1987) for the probe NBD-PC in the plasma membrane of human fibroblasts, for different radius R of the illuminated area increase linearly with the reciprocal of R ($r^2=0.973$). This enables (3B) (Appendix B) to be used for the calculation of an average radius r_m of 0.4 μm for the closed lipid domains which are postulated as existing in that membrane. Panel **B** shows the various values of the intrinsic diffusion coefficients D_0 obtained from the corresponding diffusion coefficient D_{app} measured for NBD-PC and for different values of R. D_0 was calculated by means of (8), with the above r_m value of 0.4 μm. D_0 is observed as remaining nearly constant around 1.5 10^{-9} cm^2/s, independent of R

Appendix A

Computer generation of FRAP curves

A lipid leaflet assembly is represented by a 100×100 site triangular lattice which corresponds to hexagonal packing similar to that found in a fluid lipid bilayer. Point tracers diffuse randomly in this matrix and each matrix site may either be empty or may bear an immobile obstacle or a tracer.

To generate a recovery curve, the following procedure was used:

(i) First, non-overlapping and nearly circular obstacles were generated stepwise at random in the matrix until the

desired obstacle area fraction c (expressed as the ratio of the lattice points occupied by the obstacles to the total number of lattice points in the matrix) was reached. These obstacles were given areas of 1, 7, 37, 87, 153, 297 and 595 sites (Fig. 7). For $c=0.1$, the two last obstacles were reduced to 237 and 497 sites respectively, in order to reach an area fraction (4×237/10 000 or 2×497/10 000) as close as possible to the desired value of 0.1.

In a continuous medium, the area fraction of non-overlapping randomly distributed disks cannot exceed a value of 0.55, the so-called "random parking limit" (Onoda and Liniger 1986). In the case of a lattice, this concept holds for multi-site obstacles but not for point obstacles. Accordingly, maximum area fractions of 0.7 and 0.5 were used for point and multi-site obstacles respectively.

(ii) Then, 2000 point tracers were placed at random on the obstacle-free lattice points.

(iii) After this initial building phase, all the sites of the matrix were examined sequentially. One sequential reading of the matrix determines the time-step, i.e. the time unit of the system. For the simulation of random walks, tracers were considered as behaving independently, which means that two tracers or more were allowed to occupy the same lattice site. When a tracer was found on a site i, a jump direction from i to one of the six closest neighbors j, was chosen at random. If the site j chosen for the jump was occupied by an obstacle, the jump was delayed until the next time-step. If the site j was free or occupied by a tracer, the jump could occur. If the site i bore more than one tracer, the process was repeated until all tracers were examined. Because of the finite size of the matrix, periodic boundary conditions were imposed (Eisinger et al. 1986; Saxton 1987).

Because the multi-site obstacles were not strictly circular in shape, we checked for each of them that their influence on the diffusion of tracers was identical to that of an equivalent continuous circular obstacle of radius r, expressed in lattice spacings, and calculated from the surface of the obstacle $S=\pi r^2$, expressed in number of sites. Indeed, the efficiency of a multi-site obstacle in decreasing the jump frequency of tracers is proportional to the number N_c of forbidden jumps from the obstacle-free sites in contact with the obstacle toward the sites located at the periphery of the obstacle (see insert Fig. 7). For each obstacle size, a strict linear relationship was found between N_c and the perimeter of the equivalent continuous circles ($r^2=0.999$, data not shown).

(iv) To simulate FRAP experiments under conditions of uniform disk illumination, a circular observation area of radius R was positioned at the center of the matrix. The initial fluorescence intensity I_0 measured in FRAP experiments was estimated by averaging the number of tracers located in the observation area over 100 time-steps. For the photobleaching step, all the tracers present in the observation area were deleted. Then, for the recovery step, the system was left to evolve spontaneously and for each time-step t, the number $I(t)$ of tracers present again in the observation area was calculated. 750 to 1500 time-steps were needed for a complete recovery of the tracers to be observed. For R imaging from 7 to 28 lattice spacings, a strict linear relationship ($r^2=0.997$, data not shown) was found between the number of tracers counted in the observation area (average of 10 time steps) and the number of tracers obtained by multiplying the surface of a continuous circle of the same radius by the tracer area fraction. This means that the diffusion equations which describe fluorescence recoveries under conditions of uniform disk illumination can be used to analyze the simulated recoveries, with R expressed in lattice spacings (Axelrod et al. 1976; Lopez et al. 1988).

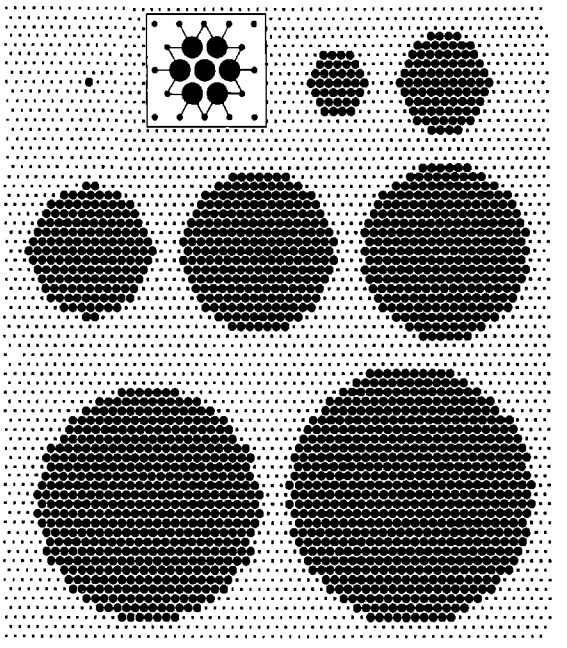

Fig. 7. Exact shape of the obstacles employed in this study. Their sizes, expressed in number of lattice spacings are from left to right: 1, 7, 37 and 87 (first row), 153, 237 and 297 (second row), 497 and 595 (third row). The insert shows the forbidden jumps (*straight lines*) which exist for tracers present on the vacant sites which are immediately adjacent to a 7-site obstacle: 18 forbidden jumps can be counted

(v) In these conditions, the fraction $f(t)$ of tracers recovered at the time-step t, which is equivalent to the fractional recovered fluorescence intensities measured in FRAP experiments, is expressed as:

$$f(t)=\frac{I(t)}{I_0} \tag{1A}$$

As shown in Fig. 8, tracer recoveries obtained in this way exhibited the typical shape of experimental FRAP recoveries. However, and because of the small number of tracers involved in one recovery process, the corresponding recovery curve was much too affected by noise to provide reliable diffusional parameters (Fig. 8A). For that reason, several distinct recoveries were accumulated and averaged. In order to give the same weight to the various tracers, each distinct recovery (indexed by i) was weighted by its initial I_{0i} value. Thus, the over-all recovery function $F(t)$ can be written:

$$F(t)=\frac{\sum_i f_i(t)\, I_{0i}}{\sum_i I_{0i}}, \tag{2A}$$

Figure 8B shows the simulated over-all recovery curve obtained in averaging 60 distinct recoveries in an obstacle-free lattice. Also shown and nearly superimposable, is the recovery curve obtained after fitting the diffusion equation to the simulated curve. In these calculations, the quality of data fitting was measured by the standard deviation σ(Lopez et al. 1988). Data fitting in Fig. 8B was achieved with a standard deviation $\sigma<0.02$ and led to a diffusion coefficient D of 0.326 a.u. and a mobile fraction M of 97% which is that expected on account of the bleaching of 3% (for $R=10$ l.s.) of the tracers added initially.

It should be stressed that for given value of R, r and c, the quality of an over-all recovery $F(t)$ depends on the number i of distinct recoveries which have been averaged. This is due to the fact that the construction of $F(t)$ implies a double averaging, one for the number of tracers present in the observation area, the other for the spatial distribution of the obstacles inside and outside the observed area. Accordingly, in an obstacle-free matrix and for $R=10$ l.s., the calculated D and M values were checked to ensure a constant value for $i>10$ and σ to reach a small and constant value around 0.02 for $i>60$. In the presence of obstacles and for $R=7$, 10–25 and 28 lattice spacings, 120, 60 and 20 distinct recoveries were required respectively for D and M to ensure constant values and σ to reach a minimum. In the following, over-all $F(t)$ recoveries were constructed on account of these numbers of distinct recoveries and in all cases, σ was less than 0.02.

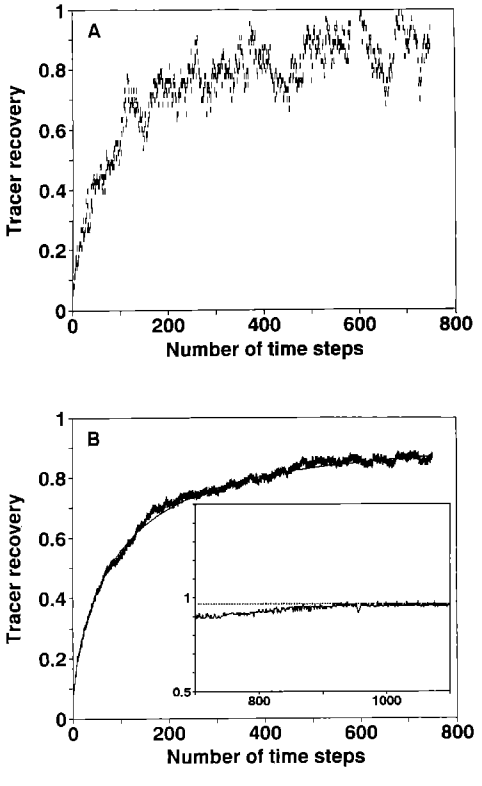

Fig. 8. Time course of tracer recovery for an individual recovery **A** and for the average of sixty recoveries **B**. Time is expressed in number of time steps. Insert shows the average recovery up to 1100 time steps. Recoveries were generated in an obstacle-free lattice with an observation area radius of 10 lattice spacings. The continuous line in **B** is the best fit of diffusion equation to the synthetic data. The final recovery was 97% of the initial tracer concentration. This does not account for an immobile lipid fraction. This originates from the finite size of the system and the bleaching conditions used which lead to the destruction of 3% of the tracers introduced at the beginning of each FRAP simulation

Appendix B

Changes in D and M above the percolation threshold*

One can reasonably assume that above an obstacle area fraction of 0.4, point obstacles tend to connect progressively and form a continuous domain enclosing small areas, like pools on the land, in which the diffusing species are free to move but from which they cannot escape (Fig. 9). This assumption stems from the two-dimensional percolation theories which indicate that above the obstacle percolation threshold, only one cluster of obstacles, infinite in size, can exist (Stauffer and Aharony 1992). As previously shown by Vaz et al. (1989) when discussing the problem of connectivity between gel and liquid lipid domains in lipid bilayers, only cavities overlapping the periphery of the observation area will contribute to both the photobleaching and recovery processes. These closed cavities display a large variety of sizes and shapes and there is no analytical expression enabling the distribution of these two parameters to be quantified. However, in the present case, this system can be analyzed in a simplified way with the following assumptions:

(i) statistically and because each recovery is an average of distinct recoveries with different random obstacle distributions, 50% of the surface of the peripheral closed cavities overlap the boundary of the observation area. As a consequence, only 50% of the tracers contained in these cavities are bleached and thus only 25% are viewed during the recovery process.
(ii) these closed cavities are considered as circular areas with the same radius r_m and centred on the boundary of the observation area (Fig. 9B). Cavities are thus included in a crown of inner radius $R-r_m$ and outer radius $R+r_m$, of surface $4\,\pi R\,r_m$.

In these conditions, the characteristic diffusion time τ_D of a given recovery can be written as:

$$\tau_D = l^2/4\,D = \pi R^2/4\,D^*_{app} = \pi R\,r_m\,(1-c)/2\,D^*_0 \qquad (1B)$$

in which D^*_{app} and D^*_0 are the relative diffusion constants obtained respectively if one considers that the recovery of tracers occurs over the full observation area of radius R or only over the real diffusion area covered by the closed cavities of average radius r_m and in which there are no obstacles to diffusion. The actual diffusion area is half that of the afore mentioned crown multiplied by the area fraction $(1-c)$ of closed cavities. From (1B) it becomes:

$$D^*_0 = [2\,r_m\,(1-c)/R]\,D^*_{app} \qquad (2B)$$

If the above assumptions are valid, application of (2B) to the diffusion coefficients obtained above the percolation threshold of point obstacles should yield D^*_0 values independent of R and c and close to 1, as is found in the absence of obstacles. This conclusion was indeed verified,

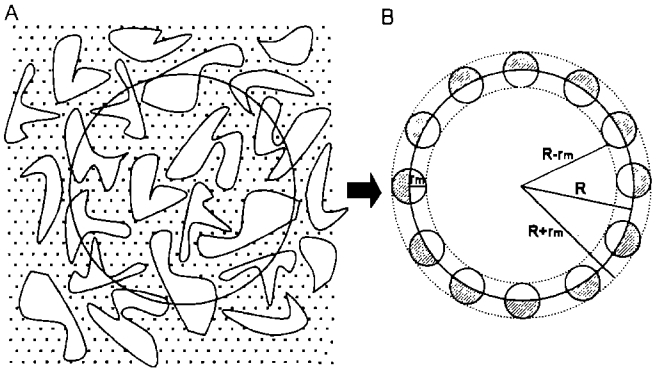

Fig. 9. Schematic drawing of the closed cavities in which the diffusion of tracers is confined above the percolation threshold when point obstacles are connected to each other and form a continuous cluster of infinite size. **A** Example of the actual size and shape distributions of these closed cavities. **B** Simplified drawing of the system in which only the closed cavities which overlap the boundary of the circular observation area of radius R are shown. These cavities are viewed as circles with the same radius r_m and centred at the periphery of the observation area. Only the tracers contained in the shaded zone contribute to the recovery

as shown in Fig. 2 for $c=0.6$ and $c=0.7$. Moreover, for a square radial distribution of bleached fluorophores in the illumination area and from the above assumptions, one can also demonstrate when $R>r_m$, that the average size r_m of the closed cavities, can be obtained from the values of M and R through the relation:

$$r_m = M\,R\,. \qquad (3B)$$

It should be stressed that the size of these cavities only depends on the distribution of point obstacles and not on R. If the above assumptions are valid, the r_m values calculated from (3B) and the mobile fractions determined for different R values and for obstacle area fractions c above the percolation threshold should be independent of R. Indeed, r_m was found to have constant values of 2.2 l.s. and 1.2 l.s. for $c=0.6$ and $c=0.7$ respectively.

References

Abney JR, Scalettar BA, Owicki JC (1989) Self diffusion of interacting membrane proteins. Biophys J 55:817–833

Almeida PFF, Vaz WLC, Thompson TE (1992) Lateral diffusion and percolation in two-phase, two-component lipid bilayers. Topology of the solid-phase domains in plane and across the lipid bilayer. Biochemistry 31:7198–7210

Axelrod D, Koppel DE, Schlessinger J, Elson E, Webb WW (1976) Mobility measurement by analysis of fluorescence photobleaching recovery kinetics. Biophys J 16:1055–1069

Blackwell MF, Whitmarsh J (1990) Effect of integral membrane proteins on the lateral mobility of plastoquinone in phosphatidylcholine proteoliposomes. Biophys J 58:1259–1271

Blaurock AE (1975) Bacteriorhodopsin: a trans-membrane pump containing alpha-helix. J Mol Biol 93:139–158

Bloom M, Evans E, Mouritsen OG (1991) Physical properties of the fluid lipid-bilayer component of cell membranes: A perspective. Q Rev Biophys 24:293–397

Bussell SJ, Hammer DA, Koch DL (1994) The effect of hydrodynamic interactions on the tracer and gradient diffusion of integral membrane proteins in lipid bilayers. J Fluid Mech 258: 167–190

Cherry RJ (1979) Rotational and lateral diffusion of membrane proteins. Biochim Biophys Acta 559:289–327

Edidin M (1987) Rotational and lateral diffusion of membrane proteins and lipids: phenomena and function. Curr Top Membr Transp 29:91–127

Eisinger J, Flores J, Petersen WP (1986) A Milling crowd model for local and long range obstructed lateral diffusion. Mobility of excimeric probes in the membrane of intact erythrocytes. Biophys J 49:987–1001

Fery-Forgues S, Fayet JP, Lopez A (1993) Drastic changes in the fluorescence properties of NBD probes with the polarity of the medium: involvement of a TICT state. J Photochem Photobiol A: Chem 70:229–243

Gulik-Krzywicki T, Seigneuret M, Rigaud JL (1987) Monomer-oligomer equilibrium of bacteriorhodopsin in reconstituted proteoliposomes. A freeze-fracture electron microscopy study. J Biol Chem 262:15580–15588

Henderson R, Unwin PNT (1975) Three-dimensional model of purple membrane obtained by electron microscopy. Nature 257: 28–32

Heyn MP, Dencher NA (1982) Reconstitution of monomeric bacteriorhodopsin into phospholipid vesicles. Methods Enzymol 88: 31–35

Heyn MP, Blume A, Rehorek M, Dencher NA (1981) Calorimetric and fluorescence depolarization studies on the lipid phase transition of bacteriorhodopsin-dimyristoylphosphatidylcholine vesicles. Biochemistry 20:7109–7115

Jähnig F (1981) Critical effects from lipid-protein interaction in membranes. I. Theoretical description. Biophys J 36:329–345

Kusumi A (1994) Confined lateral diffusion of membrane receptors as studied by single particle tracking and laser tweezers. Biophys J 66:A18

Lentz BR (1988) Organization of membrane lipids by intrinsic membrane proteins. In: Advances in membrane fluidity. Vol. 2. Aloia RC, Curtain CC, Goron LM (eds) A. R. Liss, New York, pp 141–161

Lewis BA, Engelman DM (1983) Bacteriorhodopsin remains dispersed in fluid phospholipid bilayers over a wide range of bilayer thicknesses. J Mol Biol 166:203–211

Lopez A, Dupou L, Altibelli A, Trotard J, Tocanne JF (1988) Fluorescence Recovery After Photobleaching (FRAP) experiments under conditions of uniform disk illumination: Critical comparison of analytical solutions, and a new mathematical method for calculation of diffusion coefficient D. Biophys J 53:963–970

Marsh D, Watts A (1988) Association of lipids with membrane proteins. In: Advances in membrane fluidity. Vol. 2. Aloia RC, Curtain CC, Gordon LM (eds) A. R. Liss, New York, pp 163–200

Oesterhelt D, Stoeckenius W (1974) Isolation of the cell membrane of Halobacterium halobium and its fractionation into red and purple membrane. Methods Enzymol 31:667–678

Onoda GY, Liniger EG (1986) Experimental determination of the random-parking limit in two dimensions. Phys Rev A 33: 715–716

Owicki JC, Springgate MW, McConnell HM (1978) Theoretical study of protein-lipid interactions in bilayer membranes. Proc Natl Acad Sci, USA 75:1616–1619

Peschke J, Riegler J, Möhwald H (1987) Quantitative analysis of membrane distorsions induced by mismatch of protein and lipid hydrophobic thickness. Eur Biophys J 14:385–391

Peters R, Cherry RJ (1982) Lateral and rotational diffusion of bacteriorhodopsin in lipid bilayers: Experimental test of the Saffman-Delbrück equations. Proc Natl Acad Sci, USA 79: 4317–4321

Piknova B, Perochon E, Tocanne JF (1993) Hydrophobic mismatch and long-range protein-lipid interactions in bacteriorhodopsin/phosphatidylcholine vesicles. Eur J Biochem 218:385–396

Pink DA (1985) Protein lateral movement in lipid bilayers. Simulation studies of its dependence upon protein concentration. Biochim Biophys Acta 863:9–17

Rehorek M, Dencher NA, Heyn MP (1985) Long-range lipid-protein interactions. Evidence from time-resolved fluorescence depolarization and energy-transfer experiments with bacteriorhodopsin-dimyristoylphosphatidylcholine vesicles. Biochemistry 24:5980–5988

Saxton MJ (1982) Lateral diffusion in an archipelago. Effects of impermeable patches on diffusion in a cell membrane. Biophys J 39:165–173

Saxton MJ (1987) Lateral diffusion in an archipelago: the effect of mobile obstacles. Biophys J 52:989–997

Saxton MJ (1989a) The spectrin network as a barrier to lateral diffusion in erythrocytes. A percolation analysis. Biophys J 55: 21–28

Saxton MJ (1989b) Lateral diffusion in an archipelago: distance dependence of the diffusion coefficient. Biophys J 56:615–622

Saxton MJ (1992) Lateral diffusion and aggregation. A Monte Carlo study. Biophys J 61:119–128

Scalettar BA, Abney JR (1991) Molecular crowding and protein diffusion in biological membranes. Comments Mol Cell Biophys 7:79–107

Scotto AW, Zakim D (1988) Reconstitution of membrane proteins. Spontaneous incorporation of integral membrane proteins into preformed bilayers of pure phospholipid. J Biol Chem 34: 18500–18506

Sperotto MM, Mouritsen OG (1988) Dependence of lipid membrane phase transition temperature on the mismatch of protein and lipid hydrophobic thickness. Eur Biophys J 16:1–10

Sperotto MM, Mouritsen OG (1991) Monte Carlo simulation studies of lipid order parameter profiles near integral membrane proteins. Biophys J 59:261–270

Stauffer D, Aharony A (1992) Introduction to percolation theory. Taylor and Francis, London, p 124

Tank DW, Wu ES, Meers PR, Webb WW (1982) Lateral diffusion of gramicidin *C* in phospholipid multibilayers. Effects of cholesterol and high gramicidin concentration. Biophys J 40: 129–135

Thomas JL, Holowka D, Baird B, Webb W (1994) Large-scale co-aggregation of fluorescent lipid probes with cell surface proteins. J Cell Biol 125:795–802

Tocanne JF (1992) Detection of lipid domains in biological membranes. Comments Mol Cell Biophys 8:53–72

Tocanne JF, Dupou-Cézanne L, Lopez A (1994a) Lateral diffusion of lipids in model and natural membranes. Prog Lipid Res 33:203–237

Tocanne JF, Cézanne L, Lopez A, Perochon E, Piknova B, Schram V, Tournier JF, Welby M (1994b) Lipid domains and lipid/protein interactions in biological membranes. Chem Phys Lipids (in press)

Vaz WLC, Derzko ZI, Jacobson KA (1982) Photobleaching measurements of the lateral diffusion of lipids and proteins in artificial phospholipid bilayer membranes. In: Membrane reconstitution. Poste et Nicholson (eds) Elsevier Biomedical Press, pp 83–136

Vaz WLC, Melo ECC, Thompson TE (1989) Translational diffusion and fluid domains connectivity in a two-component, two-phase phospholipid bilayer. Biophys J 56:869–876

Yeagle PL (1988) Use of NMR to study lipid phase states and protein-induced lipid domains. In: Advances in membrane fluidity. Vol. 1. Aloia RC, Curtain CC, Gordon LM (eds) A. R. Liss, New York, pp 67–295

Yechiel E, Edidin M (1987) Micrometer-scale domains in fibroblast plasma membranes. J Cell Biol 115:755–760

Wallace BA, Ravikumar K (1992) The gramicidin pore: Crystal structure of a cesium complex. Science 241:182–187